CrossMark

Deep-UV emission at 219 nm from ultrathin MBE GaN/AlN quantum heterostructures

S. M. Islam,[1,a)] Vladimir Protasenko,[1] Kevin Lee,[1] Sergei Rouvimov,[2] Jai Verma,[3,b)] Huili (Grace) Xing,[1,4,5] and Debdeep Jena[1,4,a)]
[1]Department of Electrical and Computer Engineering, Cornell University, Ithaca, New York 14853, USA
[2]Notre Dame Integrated Imaging Facility, University of Notre Dame, Notre Dame, Indiana 46556, USA
[3]Department of Electrical Engineering, University of Notre Dame, Notre Dame, Indiana 46556, USA
[4]Department of Materials Science and Engineering, Cornell University, Ithaca, New York 14853, USA
[5]Kavli Institute at Cornell for Nanoscale Science, Cornell University, Ithaca, New York 14853, USA

(Received 29 April 2017; accepted 18 August 2017; published online 30 August 2017)

Deep ultraviolet (UV) optical emission below 250 nm (∼5 eV) in semiconductors is traditionally obtained from high aluminum containing AlGaN alloy quantum wells. It is shown here that high-quality epitaxial ultrathin binary GaN quantum disks embedded in an AlN matrix can produce efficient optical emission in the 219–235 nm (∼5.7–5.3 eV) spectral range, far above the bulk bandgap (3.4 eV) of GaN. The quantum confinement energy in these heterostructures is larger than the bandgaps of traditional semiconductors, made possible by the large band offsets. These molecular beam epitaxy-grown extreme quantum-confinement GaN/AlN heterostructures exhibit an internal quantum efficiency of 40% at wavelengths as short as 219 nm. These observations together with the ability to engineer the interband optical matrix elements to control the direction of photon emission in such binary quantum disk active regions offer unique advantages over alloy AlGaN quantum well counterparts for the realization of deep-UV light-emitting diodes and lasers. *Published by AIP Publishing*. [http://dx.doi.org/10.1063/1.5000844]

The ruggedness, portability, high-efficiency, and microfabrication benefits of solid-state semiconductor light sources over conventional lamps became clear in the last decade for visible wavelengths in the solid-state lighting revolution and gave rise to several new applications. A similar revolution is expected in the deep-ultraviolet (UV) spectrum. Semiconductor light sources such as Light-Emitting Diodes (LEDs) and Lasers in the deep ultraviolet (UV) spectrum have versatile applications in water and air purification, in healthcare applications of bio-photonic diagnostics and sterilization, in food preservation, in security and environmental monitoring, and in industrial curing. The semiconductor material substrate of choice for deep-UV photonic devices is direct-bandgap AlN with an energy bandgap of ∼6.02 eV (205 nm),[1] and the active regions where photons are produced are various ternary compositional alloys of AlN with GaN of bandgap ∼3.4 eV (365 nm).

For deep-UV LEDs, quantum well (QW) active regions composed of AlGaN have been used to push the interband optical transition to high energies.[2–5] The internal quantum efficiency (IQE) in high Al containing AlGaN quantum wells (QWs)/barrier structures is limited by the quantum confined Stark effect (QCSE),[6–8] edge emission due to valence band structure re-ordering,[9–11] combined with material defect (e.g., dislocation) induced non-radiative recombination. Compositional fluctuations of Al and Ga concentrations in ternary AlGaN alloy layers degrade efficient optical emission in the deep-UV range[12] and together with the other effects degrade the LED efficiency.

Distinct from the alloy AlGaN layers, deep-UV emission down to 224 nm has been achieved in binary GaN/AlN heterostructures.[13–17] As a significant advantage, the polarization of the emitted photons in ultrathin GaN QWs and quantum dots/disks (QDs) is perpendicular to the c axis, making them propagate parallel to the c-axis;[9,11] this surface emission property is highly favorable for light extraction.

We recently demonstrated deep UV LEDs[18–20] emitting as short as 232 nm by incorporating 2 monolayer (ML) thick GaN QDs in AlN barriers. As the height of the QD reduces and the oscillator strength increases,[21] the radiative lifetime decreases significantly, increasing the internal quantum efficiency. Shortening the emission wavelength even deeper below 230 nm by utilizing GaN QDs embedded in AlN barriers will further enable applications in sensing and toxic gas detection applications. Tunable sub-230 nm deep-UV emission was demonstrated by molecular beam epitaxy (MBE) growth of 2 ML GaN QDs using a modified Stranski-Krastanov (m-SK) growth mode.[16] The m-SK technique uses thermal annealing of the 2 ML GaN quantum well structure sandwiched between AlN barriers.[22] In this letter, we present an *alternative* approach to realize tunable sub-230 nm emission with higher internal quantum efficiency using the SK growth mode of 2 ML GaN QD structures by MBE. Unlike the earlier work based on the m-SK mode, control of the emission wavelength is achieved by changing the Ga/N ratio in a Nitrogen-rich growth regime that ensures dot/disk formation. This SK growth mode for GaN QDs enables us to achieve shorter wavelength (219 nm with SK compared to 222 nm with m-SK) with higher internal quantum efficiency (40% with SK compared to 36% with m-SK).

The samples studied were grown using a Veeco Gen-930 plasma assisted MBE system on 1 μm thick AlN templates on sapphire of threading dislocation density $\sim 10^{10}\,cm^{-2}$. After standard solvent cleaning, the samples were loaded in the

a)Authors to whom correspondence may be addressed: smislam@cornell.edu; djena@cornell.edu
b)Presently at Intel Corporation, Oregon, USA.

MBE chamber and outgassed for 7 h at 200 °C followed by ∼2 h at 450 °C. Prior to the epitaxy of heterostructures discussed in this work, calibration growths were performed to identify the most suitable AlN barrier thickness, the GaN annealing time, and the growth rate for the most intense deep-UV emission. Based on these studies, three samples containing 2 ML GaN/4 nm AlN barrier heterostructures shown in Fig. 1(a) were grown under conditions indicated in Fig. 1(b). The substrate thermocouple temperature was 730 °C throughout the growths, with an Al flux of 1×10^{-7} Torr beam equivalent pressure. The RF plasma power of 275 W with 1.2 sccm flow led to an effective nitrogen BEP (Beam equivalent pressure) of 1×10^{-7} Torr (at a chamber pressure of $\sim 2 \times 10^{-5}$ Torr). The Ga flux was varied for the three samples to change the size of the QDs to tune the UV emission wavelength.

The active region contained 10 periods of the GaN/AlN heterostructure grown on a 30 nm AlN buffer layer as shown in Fig. 1(a). The 4 nm AlN barriers were grown using migration enhanced epitaxy (MEE)[23] to ensure a smooth heterointerface between AlN and GaN by avoiding excess Al.

Because of the strong preference of Al incorporation over Ga, an Al-free surface is necessary to incorporate ultra-thin GaN QDs in the AlN matrix. RHEED oscillations[24] were used to precisely determine and control the growth rate at ∼0.3 ML/s and to maintain desired stoichiometry for AlN and GaN. The 2 ML GaN QDs were grown in N-rich conditions by opening the Ga and N shutters simultaneously for 7 s ensuring the SK growth mode. A growth interrupt (anneal) of 18 s was introduced after each GaN layer deposition to assist island formation by layer decomposition. The Ga/N ratio was varied from 0.88 (A) → 0.75 (B) → 0.6 (C) for the three samples. Figure 1(b) shows the flux-time diagram for 1 complete cycle of the quantum dot superlattice active region.

Figure 1(c) shows the measured triple-axis X-Ray Diffraction (002) ω-2θ spectrum. The AlN peak in all samples is similar to the control substrate which was 1 μm AlN on 430 μm sapphire. All three GaN/AlN UV emitter samples show satellite fringes due to reflections from the heterointerfaces confirming periodic GaN/AlN heterostructures. The fringes for samples B and C were more prominent than sample A, suggesting sample A to be more disk-like and B/C to be more well-like quantum structures.[25,26] QD-like features cause diffuse scattering of the XRD beam preventing well defined satellite peaks.[25] As the Ga/N ratio is reduced from 0.88 to 0.6, reflection from the well-like GaN planes produces constructive interference[26] and strong XRD fringes. Figures 2(a) and 2(b) show Z-contrast Scanning Transmission-Electron Microscopy (STEM) images of sample A which was grown with a 0.88 Ga/N ratio. Sharp heterointerfaces were observed between GaN and AlN suggesting no intermixing to form AlGaN alloy. The existence of 1–2 ML GaN QDs is clearly indicated in Fig. 2(b). Also in some places, the GaN layer was completely absent. The image indicates that by growing GaN under N-rich conditions, the effective QD thickness can be varied between 0 and 2 monolayers.

Figure 3(a) shows the measured 5 K photoluminescence (PL). A pulsed Excimer laser ($\lambda = 157$ nm, 5 ns pulse duration, 600 μJ/pulse energy, 157 Hz repetition rate, 300 μm $\times$ 300 μm spot size corresponding to a steady state carrier density of $\sim 5 \times 10^{19}$ cm^{-3}) was used for PL excitation. Sample A with the highest Ga/N ratio of ∼0.9 shows a peak

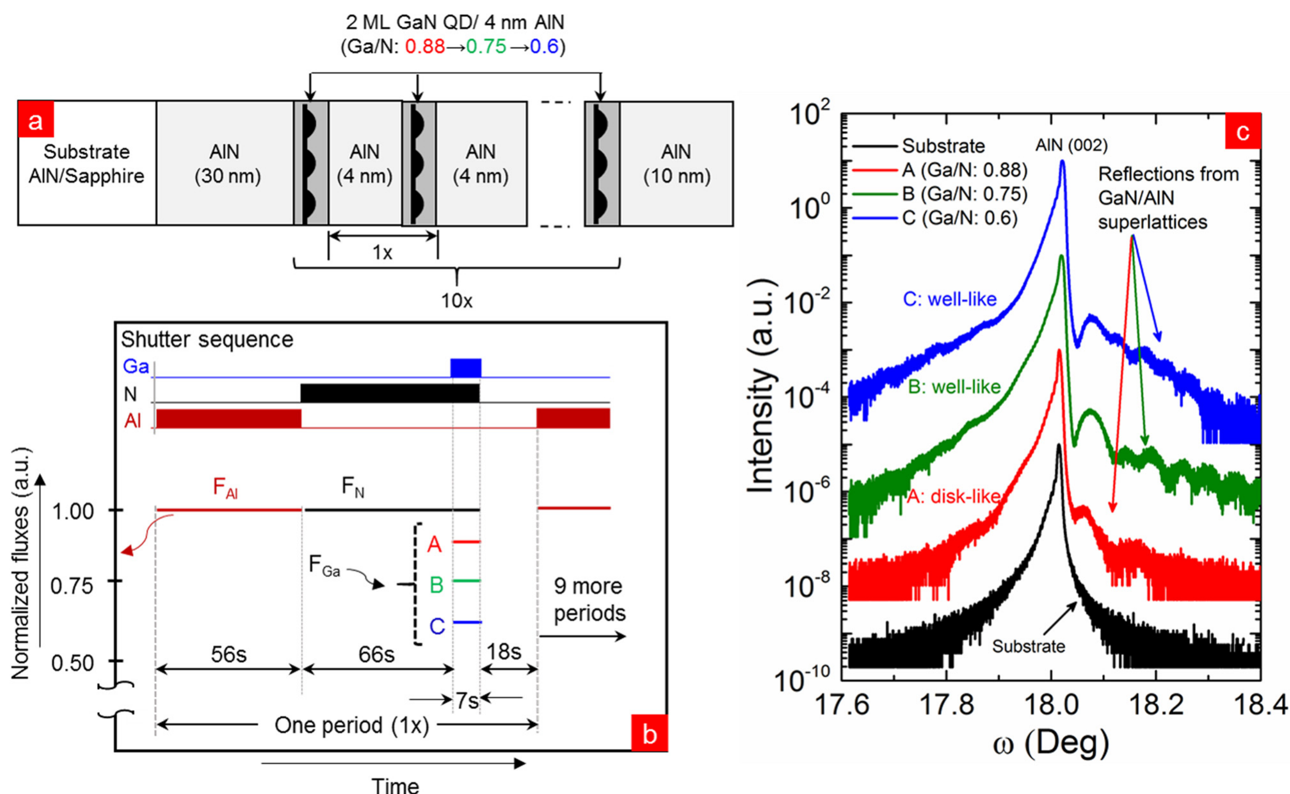

FIG. 1. (a) Schematic of the structure with 10 periods of ultra-thin GaN QDs in AlN barriers, (b) MBE growth diagram showing shutter sequence and relative III-V fluxes for 1 period of the growth, and (c) high-resolution-x-ray diffraction (HR-XRD) ω-2θ scans showing signature of QD formation for sample A.

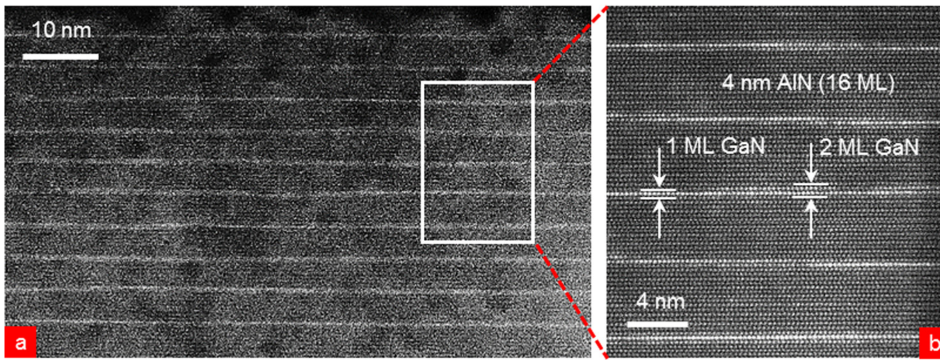

FIG. 2. Z-contrast STEM images for sample A: (a) large area scan showing uniform distribution of the 10 periods of GaN/AlN heterostructures and (b) zoomed-in image showing the presence of 1 ML and 2 ML GaN QDs separated by 4 nm AlN.

PL emission at 234 nm, sample B (Ga/N: 0.75) at 222 nm, and sample C with the lowest Ga/N ratio of 0.6 exhibits a 219 nm PL peak at 5 K. This is the *highest* reported emission energy to-date using GaN as the light emitting material. Temperature-dependent PL measurements showed that at 300 K the PL peak wavelength red-shifted by ~4 nm consistent with a Varshni trend. The measured PL peak positions were compared with a Schrodinger-Poisson simulation using SiLENSe software; an example energy-band diagram is shown in Fig. 3(b). The effective GaN thicknesses for the three samples to match the peak PL wavelength with experiment were ~1.4 ML (A), 1 ML (B), and 0.8 ML (C). Thus, the emission wavelength can be reproducibly controlled by choosing the appropriate Ga/N ratio. The absolute integrated PL intensity was found to decrease at the shorter wavelengths with lowering the Ga/N ratio. This is expected because of the reduction of the total GaN volume at higher N-rich growth conditions. The high electron-hole overlap seen in Fig. 3(b) calculated for the 0.8 ML effective GaN thickness indicates robustness to the quantum-confined Stark effect and leads to an interband transition wavelength of 219 nm (5.67 eV) for deep-UV emission, consistent with the experimental observation.

The PL linewidth is a measure of the thickness fluctuations of the GaN layers. For example, the average thickness of the GaN layers for each of the samples in Fig. 3(a) is 1.4 ML (A), 1 ML (B), and 0.8 ML (C) as mentioned before. Based on the STEM image in Fig. 2(b), the thickest GaN layer region in the samples is 2 ML. Therefore, the thickness fluctuation (Δz) for the three samples is ~0.6 ML (A), ~1 ML (B), and ~1.2 ML (C), respectively. The broadening is estimated using the formula $(dE_0/dz)\cdot\Delta z$ where dE_0/dz is the differential change of the eigenvalue energies calculated at the effective GaN thicknesses for the three samples. The simulation tool SiLENSe is used to calculate dE_0/dz for each of the samples. Based on this analysis, the calculated broadening due to the thickness fluctuation is 16 nm (A), 30 nm (B), and 36 nm (C) which are higher than the measured values of 9 nm (A), 20 nm (B), and 19 nm (C). This qualitative agreement shows the correct trend and order of magnitude, but to obtain quantitative agreement it is necessary to incorporate the size variations with full-bandstructure models[17] that is not attempted here. Furthermore, the symmetrical PL lineshape of disk-like sample A and the asymmetrical lineshapes of well-like samples B/C with respect to photon energy show good agreement with the models discussed in Ref. 17. The PL lineshapes are guided by the distribution of joint density of states and therefore different for the well-like and the disk-like samples.

Figure 4(a) shows the temperature-dependent integrated PL spectra which are indicative of the internal quantum efficiency (IQE). The IQE estimated from the 300 K/5 K ratio was 20% for sample A grown at a Ga/N ratio of 0.88. The IQE went up to 40.2% for sample C with a Ga/N ratio of 0.6.

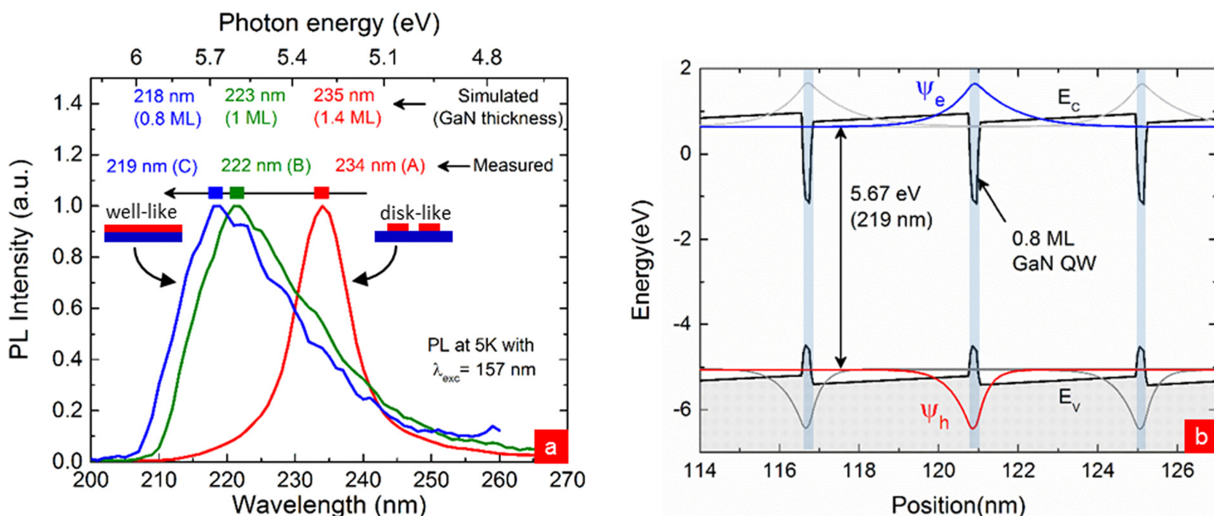

FIG. 3. (a) Normalized measured photoluminescence (5 K) and absorption (300 K) spectra showing tunable deep-UV emission down to 219 nm. The average thickness of GaN layers were extracted from simulation. (b) Simulated energy-band diagram for 219 nm emission.

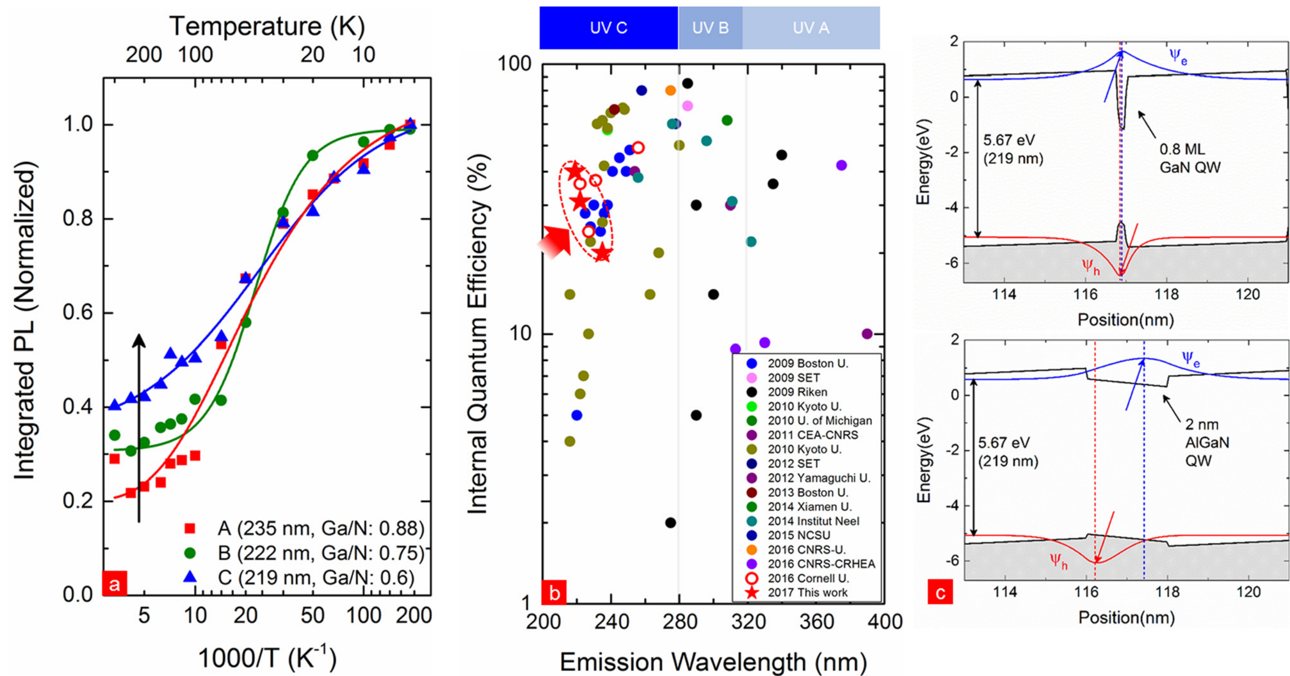

FIG. 4. (a) Estimation of IQE from temperature dependent integrated PL spectra (solid lines are shown as a guide to the reader), (b) comparison of measured IQE with AlGaN based QWs, (c) enhancement of IQE using GaN QWs due to the reduced quantum-confined Stark effect.

The increase in IQE is explained by the reduction of the QCSE. These IQE values can be a consequence of very high photo-excited carrier densities in the order of $\sim 10^{20}\,\mathrm{cm}^{-3}$ which can cause over-estimation due to saturation of SRH (Shockley-Read-Hall) non-radiative recombination centers or under-estimation due to the Auger effect. A detailed optical power density dependent IQE measurement needs to be performed to obtain the IQE vs carrier density map which has not been performed in the current work. Figure 4(c) (top & bottom) compares the energy band diagrams and electronic states of an ultrathin GaN QW/QD with a corresponding AlGaN QW with the *same* photon emission energy. The significantly higher overlap of the electron/hole wavefunctions indicates a higher oscillator strength, which should translate to a higher IQE.

Figure 4(b) shows the measured IQE for the heterostructures reported in this work in comparison to those reported in the literature over the range of 200–400 nm.[27–41] To increase the photon energy in traditional AlGaN based thick (>2 nm) QW active regions, the Al-content in the AlGaN is typically increased. The high QCSE and lower band offset induced carrier leakage into the barriers reduce the IQE of AlGaN active regions. Beyond an Al content of 40%,[9] the optical matrix element leads to edge-emission from AlGaN QWs. On the contrary, for the GaN based structures shown in this work, the IQE is found to *increase* at shorter wavelength emission. This is achieved because the reduction of the GaN QW/QD thickness enhances the overlap integral, reversing the trend of decreasing IQE at shorter wavelengths. Furthermore, the emission matrix element is converted to surface-emission,[13] which is highly desirable for light extraction.

In conclusion, ultrathin (1–2ML) GaN dots/disks in the AlN matrix were demonstrated to be capable of controllable emission in the 219–235 nm range by engineering the quantum confinement during the MBE growth, showing the shortest wavelength emission till date at 219 nm (~5.7 eV) from binary GaN active regions. An IQE of 40% at an emission wavelength of 219 nm was measured, which is more than 2X higher than the highest prior reported AlGaN QW based heterostructures at comparable short deep-UV wavelengths. Together with the reduced QCSE and the surface emission, the use of the extreme quantum confinement binary GaN QW/QD active regions offers a compelling approach for efficient deep UV light emitters.

This work was supported in part by a NSF DMREF Grant No. 1534303 and an AFOSR grant.

[1] M. Feneberg, R. A. R. Leute, B. Neuschl, and K. Thonke, Phys. Rev. B **82**, 075208 (2010).
[2] T. D. Moustakas, "Gallium nitride II," in *Semiconductors and Semimetals*, edited by J. I. Pankove and T. D. Moustakas (Academic, New York, 1999), Vol. 57, pp. 33–121.
[3] A. Khan, K. Balakrishnan, and T. Katona, Nat. Photonics **2**, 77 (2008).
[4] C. Pernot, M. Kim, S. Fukahori, T. Inazu, T. Fujita, Y. Nagasawa, A. Hirano, M. Ippommatsu, M. Iwaya, and S. Kamiyama, Appl. Phys. Express **3**, 061004 (2010).
[5] M. Kneissl, T. Kolbe, C. Chua, V. Kueller, N. Lobo, J. Stellmach, A. Knauer, H. Rodriguez, S. Einfeldt, Z. Yang, N. M. Johnson, and M. Weyers, Semicond. Sci. Technol. **26**, 014036 (2011).
[6] D. A. B. Miller, D. S. Chemla, T. C. Damen, A. C. Gossard, W. Wiegmann, T. H. Wood, and C. A. Burrus, Phys. Rev. Lett. **53**, 2173 (1984).
[7] T. Takeuchi, S. Sota, M. Katsuragawa, M. Komori, H. Takeuchi, H. Amano, and I. Akasaki, Jpn. J. Appl. Phys., Part 2 **36**, L382 (1997).
[8] F. Bernardini and V. Fiorentini, Phys. Status Solidi A **190**, 65 (2002).
[9] K. B. Nam, J. Li, M. L. Nakarmi, J. Y. Lin, and H. X. Jiang, Appl. Phys. Lett. **84**, 5264 (2004).
[10] J. E. Northrup, C. L. Chua, Z. Yang, T. Wunderer, M. Kneissl, N. M. Johnson, and T. Kolbe, Appl. Phys. Lett. **100**, 021101 (2012).
[11] C. Liu, Y. K. Ooi, S. M. Islam, J. Verma, H. Xing, D. Jena, and J. Zhang, Appl. Phys. Lett. **110**, 071103 (2017).
[12] A. Bhattacharyya, T. D. Moustakas, L. Zhou, D. J. Smith, and W. Hug, Appl. Phys. Lett. **94**, 181907 (2009).
[13] Y. Taniyasu and M. Kasu, Appl. Phys. Lett. **99**, 251112 (2011).

[14]J. Renard, P. K. Kandaswamy, E. Monroy, and B. Gayral, Appl. Phys. Lett. **95**, 131903 (2009).
[15]C. Himwas, M. den Hertog, E. Bellet-Amalric, R. Songmuang, F. Donatini, L. Si Dang, and E. Monroy, J. Appl. Phys. **116**, 023502 (2014).
[16]S. M. Islam, V. Protasenko, S. Rouvimov, H. Xing, and D. Jena, Jpn. J. App. Phys., Part 1 **55**, 05FF06 (2016).
[17]D. Bayerl, S. M. Islam, C. M. Jones, V. Protasenko, D. Jena, and E. Kioupakis, Appl. Phys. Lett. **109**, 241102 (2016).
[18]J. Verma, P. Kandaswamy, V. Protasenko, A. Verma, H. Xing, and D. Jena, Appl. Phys. Lett. **102**, 041103 (2013).
[19]J. Verma, S. M. Islam, V. Protasenko, P. Kumar Kandaswamy, H. (Grace) Xing, and D. Jena, Appl. Phys. Lett. **104**, 021105 (2014).
[20]S. M. Islam, K. Lee, J. Verma, V. Protasenko, S. Rouvimov, H. (Grace) Xing, and D. Jena, Appl. Phys. Lett. **110**, 041108 (2017).
[21]S. Kako, M. Miyamura, K. Tachibana, K. Hoshino, and Y. Arakawa, Appl. Phys. Lett. **83**, 984 (2003).
[22]B. Daudin, F. Widmann, G. Feuillet, Y. Samson, M. Arlery, and J. L. Rouvière, Phys. Rev. B **56**, R7069 (1997).
[23]Y. Horikoshi, M. Kawashima, and H. Yamaguchi, Jpn. J. Appl. Phys., Part 1 **27**(2), 169–179 (1988).
[24]T. Sakamoto, H. Funabashi, K. Ohta, T. Nakagawa, N. J. Kawai, T. Kojima, and Y. Bando, Superlattice. Microstruct. **1**, 347–352 (1985).
[25]A. Darhuber, J. Stangl, V. Holy, G. Bauer, A. Krost, M. Grundmann, D. Bimberg, V. M. Ustinov, P. S. Kop'ev, A. O. Kosogov, and P. Werner, Thin Film Solids **306**, 198–204 (1997).
[26]T. Passow, K. Leonardi, A. Stockmann, H. Heinke, and D. Hommel, J. Phys. D: Appl. Phys. **32**, A42–A46 (1999).
[27]S. Watanabe, N. Yamada, M. Nagashima, Y. Ueki, C. Sasaki, Y. Yamada, T. Taguchi, K. Tadatomo, H. Okagawa, and H. Kudo, Appl. Phys. Lett. **83**, 4906 (2003).
[28]M. Shatalov, J. Yang, W. Sun, R. Kennedy, R. Gaska, K. Liu, M. Shur, and G. Tamulaitis, J. Appl. Phys. **105**, 073103 (2009).
[29]H. Hirayama, S. Fujikawa, N. Noguchi, J. Norimatsu, T. Takano, K. Tsubaki, and N. Kamata, Phys. Status Solidi A **206**(6), 1176–1182 (2009).
[30]T. Oto, R. G. Banal, K. Kataoka, M. Funato, and Y. Kawakami, Nat. Photonics **4**, 767–770 (2010).
[31]P. Bhattacharya, M. Zhang, and J. Hinckley, Appl. Phys. Lett. **97**, 251107 (2010).
[32]Z. Gacevic, A. Das, J. Teubert, Y. Kotsar, P. K. Kandaswamy, T. Kehagias, T. Koukoula, P. Komninou, and E. Monroy, J. Appl. Phys. **109**, 103501 (2011).
[33]R. G. Banal, M. Funato, and Y. Kawakamib, Appl. Phys. Lett. **99**, 011902 (2011).
[34]M. Shatalov, W. Sun, A. Lunev, X. Hu, A. Dobrinsky, Y. Bilenko, J. Yang, M. Shur, R. Gaska, C. Moe, G. Garrett, and M. Wraback, Appl. Phys. Express **5**, 082101 (2012).
[35]H. Murotani, D. Akase, K. Anai, Y. Yamada, H. Miyake, and K. Hiramatsu, Appl. Phys. Lett. **101**, 042110 (2012).
[36]E. F. Pecora, W. Zhang, A. Yu. Nikiforov, J. Yin, R. Paiella, L. D. Negro, and T. D. Moustakas, Appl. Phys. Lett. **113**, 013106 (2013).
[37]T. Sano, T. Doi, S. A. Inada, T. Sugiyama, Y. Honda, H. Amano, and T. Yoshino, Jpn. J. Appl. Phys., Part 1 **52**, 08JK09 (2013).
[38]W. Yang, J. Li, Y. Zhang, P. K. Huang, T. C. Lu, H. C. Kuo, S. Li, X. Yang, H. Chen, D. Liu, and J. Kang, Sci. Rep. **4**, 5166 (2014).
[39]Z. Bryan, I. Bryan, J. Xie, S. Mita, Z. Sitar, and R. Collazo, Appl. Phys. Lett. **106**, 142107 (2015).
[40]J. Sellés, C. Brimont, G. Cassabois, P. Valvin, T. Guillet, I. Roland, Y. Zeng, X. Checoury, P. Boucaud, M. Mexis, F. Semond, and B. Gayral, Sci. Rep. **6**, 21650 (2016).
[41]J. Brault, S. Matta, T. H. Ngo, M. Korytov, D. Rosales, B. Damilano, M. Leroux, P. Vennéguès, M. Al Khalfioui, A. Courville, O. Tottereau, J. Massies, and B. Gil, Jpn. J. Appl. Phys., Part 1 **55**, 05FG06 (2016).